Depletion potential near curved surfaces

Weihua Li and H. R. Ma
Institute of Theoretical Physics, Shanghai Jiao Tong University, Shanghai 200240, China
(Received 6 May 2002; revised manuscript received 6 June 2002; published 30 December 2002)

We examine the depletion potential and force of a hard-sphere fluid on a single big hard sphere, located inside or outside of a hard spherical cavity, by Monte Carlo simulations to the hard-sphere fluid. The depletion potential is determined by the acceptance ratio method, while the force on the big sphere is obtained by two methods: numerical differentiation of the depletion potential and integration of the contact density of the fluid at the surface of the big sphere. The results are in excellent agreement with those obtained by density functional theory presented by Roth *et al.*

DOI: 10.1103/PhysRevE.66.061407 PACS number(s): 82.70.Dd

I. INTRODUCTION

Depletion forces in colloidal suspensions and in polymer-colloid systems are of long-standing and continuing interest [1–16] in the last few decades. Asakura and Oosawa (AO) [1] first described this depletion mechanism, suggesting that it would drive phase separation in colloid-polymer mixtures. Using excluded volume arguments they calculated the depletion force between two hard spheres of radius R_b in a fluid of small hard spheres of radius R_s, and showed that the force is attractive for all separations less than $2R_s$ and is zero for larger separations. In the past years, a lot of experimental works were available on the subject by scattering methods [6–8]. There were also direct methods used to determine the depletion potential between a colloidal hard sphere and a hard wall, between a hard sphere and a spherical surface induced by smaller colloidal particles [9,10], and by nonadsorbing polymers [8]. In particular, Dinsmore *et al.* [10] have employed video microscopy to probe the behavior of a microscopic sphere trapped inside of a rigid, phospholipid vesicle. Theoretical investigations beyond the simple free volume argument are density functional theory (DFT) calculations by Götzelmann *et al.* [11], the virial expansion by Mao *et al.* [12], and simulations [13,14]. Attard [2] has derived an exact expression for the depletion force in terms of the equilibrium number density profile of the fluid from the density functional theory. By using the exact force expression Götzelmann *et al.* [11] have constructed a series of approximate expressions of the depletion force: the AO approximation, the Derjaguin approximation, and the wedge approximation with increasing complexity and accuracy. In Ref. [4] a very accurate new approach based on the density functional theory developed by Rosenfeld [3] for calculating the depletion potential in a hard-sphere mixture is presented by Götzelmann *et al.* They obtained some perfect theoretical results of the depletion potential on a single big hard sphere inside or outside of a hard spherical cavity [5].

Simulations of the depletion potential and force between (1) a macrosphere and a hard wall, and (2) a pair of macrospheres for binary hard-sphere mixtures have was performed by Dickman [14]. We shall study here, by means of the Monte Carlo simulation method together with the acceptance ratio method (ARM) introduced by Bennett [17], the depletion potential and force between a big hard sphere of radius R_b and the spherical cavity in a system of hard-sphere fluid. The volume fraction of the fluid is η_s [defined as $\eta_s = N\frac{4}{3}\pi R_s^3/(V-4\pi R_b^3/3)$, where V is the total volume of the simulating cell]. The radius of the spherical cavity is R_c, and the big hard sphere can be inside or outside of the cavity. By simulating directly the free energy differences of systems with different separations between the big sphere and the spherical surface, we extract the depletion potential and force. As a comparison, the depletion force is also calculated by the use of the exact expression of [11]; we refer to this method as the density integration method (DIM). The ARM does not need the knowledge of density profiles of the fluid, while the calculation by using the exact expression, the DIM, do. As is well known, in a system that has a lack of symmetry, accurate determination of the density profile needs to generate a large number of configurations, which is very time consuming. We will see that the ARM is superior compared to the DIM in the calculation of both the depletion potential and the depletion force.

The paper is organized as follows. In Sec. II we derive the expression of the depletion potential and force of the system from the AO approximation. The implementation of the ARM in this system is given in Sec. III. In Sec. IV we give the details of the Monte Carlo (MC) simulation, together with results and discussions.

II. DEPLETION POTENTIAL AND FORCE IN AO APPROXIMATION

The model system under research is a big hard sphere of radius R_b in a fluid of small hard-sphere particles of radius R_s inside or outside of a rigid spherical cavity of radius R_c [as shown in Fig. 1(a) and Fig. 1(b)]. The force on the big sphere exerted by the fluid in the presence of rigid spherical cavity, the so-called depletion force, can be expressed as [11]

$$\beta \mathbf{f}(h) = -\int_S dA \rho(\mathbf{R})\hat{\mathbf{n}}, \tag{1}$$

where $\beta=(k_BT)^{-1}$. The integration is over the surface S of a sphere of radius R_b+R_s spanned from the center of the big sphere; $\hat{\mathbf{n}}$ is the unit normal vector pointing outwards from the big sphere. The force depends on the distribution of the equilibrium contact number density of the fluid, which is fixed by the external potential due to the cavity and the big hard sphere itself. In the absence of the cavity or other ob-

 ©2002 The American Physical Society

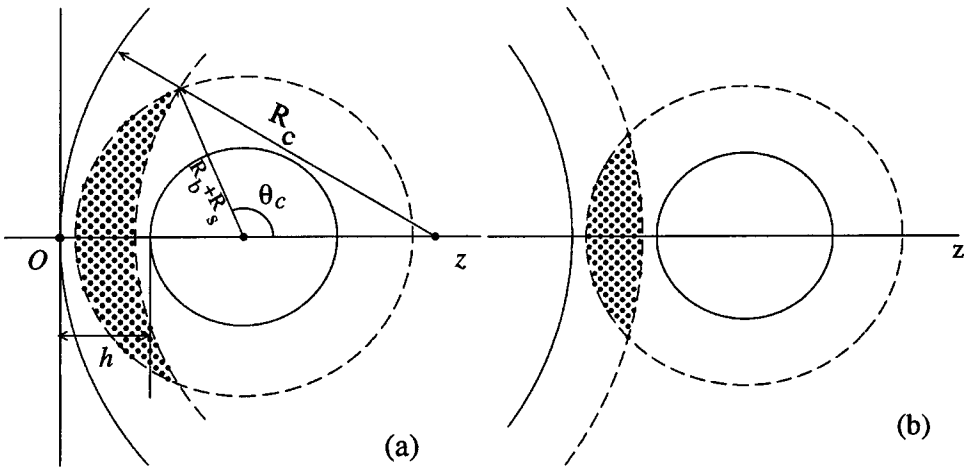

FIG. 1. Schematic drawing of the two kinds of systems studied in this paper. A fixed hard sphere with radius R_b, in a fluid of smaller hard spheres with radius R_s, located (a) inside or (b) outside of a spherical cavity of radius R_c. The z axis is the axis connecting the centers of cavity and the big sphere h is the distance between the vesicle wall and the big sphere surface along the z axis. θ_c is the value of the polar angle beyond which is the excluded volume (dotted areas) of small spheres. For reasons of clarity the schematic drawings correspond to $R_b=1.25R_s$ and $R_c=5R_s$.

stacles, this density profile is symmetric around the big sphere so that this force vanishes. The reduction of symmetry by the presence of the rigid cavity gives rise to a nonzero force $f_z(h)$, where z is along the h direction. However, the system has rotational symmetry around the z axis, so that the density profile has the same symmetry and Eq. (1) leads to [14]

$$\beta f_z(h)=-2\pi(R_b+R_s)^2\int_0^\pi d\theta\sin\theta\cos\theta\rho(\theta), \quad (2)$$

where θ is the polar angle with respect to the z axis (see Fig. 1), and $\rho(\theta)$ is the contact number density of the fluid on the surface of the fixed big sphere. It is obvious that in this case $f_x=f_y=0$. Equation (2) can be rewritten as [11]

$$\beta f_z(h)=-2\pi(R_b+R_s)^2\int_{\pi/2}^\pi d\theta\sin\theta(-\cos\theta)\Delta\rho(\theta). \quad (3)$$

Here $\Delta\rho(\theta)=\rho(\theta)-\rho(\pi-\theta)$ is the difference between the contact densities around the left $\rho(\theta)$ and the right $\rho(\pi-\theta)$ hemisphere of the big sphere.

The AO approximation, proposed by Asakura and Oosawa [1], assumes that the density profile takes the bulk value in the part where the small spheres can be accommodated, and is zero in the part where the small spheres cannot enter. This approximation is only justified for very low bulk densities of the fluid. Under this approximation, the depletion force can be written as

$$\beta f_{\mathrm{AO}}^{\mathrm{CS}}(h)=-2\pi(R_b+R_s)^2\int_{\theta_c}^\pi d\theta\sin\theta(-\cos\theta)\Delta\rho(\theta), \quad (4)$$

where θ_c is the value of θ when the small sphere just contacts with both the big sphere and the cavity surface, $\Delta\rho(\theta)=-\rho_s$, and ρ_s is the bulk number density of the small sphere fluid. According to simple geometries, the cosine value of the angle θ_c (see Fig. 1) is

$$\cos\theta_c=\frac{(R_b+R_s)^2+(R_c-h-R_b)^2-(R_c-R_s)^2}{2(R_b+R_s)(R_c-h-R_b)} \quad (5)$$

for the case of the big sphere inside the cavity, and

$$\cos\theta_c=-\frac{(R_c+h+R_b)^2+(R_b+R_s)^2-(R_c+R_s)^2}{2(R_c+h+R_b)(R_b+R_s)} \quad (6)$$

for the case of the big sphere outside the cavity. Inserting Eq. (5) and Eq. (6) into Eq. (4), we have

$$\beta f_{\mathrm{AO}}^{\mathrm{CS}}(h)=-2\pi\rho_s\Theta(2R_s-h)\times\frac{(R_c-h/2)(R_c-R_s-R_b-h/2)}{(R_c-R_b-h)^2}\times\left(R_b+\frac{1}{2}h\right)\times(2R_s-h) \quad (7)$$

and

$$\beta f_{\mathrm{AC}}^{\mathrm{CS}}(h)=-2\pi\rho_s\Theta(2R_s-h)\times\frac{(R_c+h/2)(R_c+R_s+R_b+h/2)}{(R_c+R_b+h)^2}\times\left(R_b+\frac{1}{2}h\right)\times(2R_s-h), \quad (8)$$

respectively, where $\Theta(r)$ is the Heaviside step function. In the limit of $R_c\to\infty$, the depletion force, Eqs. (7) and (8), becomes

$$\beta f_{\mathrm{AO}}^{\mathrm{WS}}(h)=-2\pi\rho_s\Theta(2R_s-h)\left(R_b+\frac{1}{2}h\right)(2R_s-h), \quad (9)$$

which is the depletion force on the big sphere in the presence of a planar hard wall located a distance h apart.

By integrating the depletion force, the associated depletion potential on a big sphere inside and outside of a cavity (cavity sphere model) is, respectively,

$$\beta V_{\mathrm{AO}}^{\mathrm{CS}} = -\frac{1}{3}\pi\rho_s\Theta(2R_s-h) \times\frac{(3R_b+R_s+h)R_c-(R_bR_s+R_sh+R_bh+h^2/4)}{R_c-h-R_b} \times(2R_s-h)^2 \tag{10}$$

and

$$\beta V_{\mathrm{AO}}^{\mathrm{CS}} = -\frac{1}{3}\pi\rho_s\Theta(2R_s-h) \times\frac{(3R_b+R_s+h)R_c+(R_bR_s+R_sh+R_bh+h^2/4)}{R_c+h+R_b} \times(2R_s-h)^2. \tag{11}$$

Moreover, the potential for a big sphere and a hard planar wall (wall sphere model) is

$$\beta V_{\mathrm{AO}}^{\mathrm{WS}} = -\frac{1}{3}\pi\rho_s\Theta(2R_s-h)(2R_s-h)^2(3R_b+R_s+h). \tag{12}$$

The potential zero is set so far away at the place where two obstacles are separated that the hard-sphere fluid density between them tends to bulk density for the wall sphere model, and at the center of the cavity where the center of the big sphere is located for the cavity sphere model, respectively.

III. SIMULATION OF THE DEPLETION POTENTIAL

Consider two systems of hard-sphere fluid in an external potential characterized by a rigid cavity and a big hard sphere inside or outside of the hard cavity, with different separations between the big hard sphere and the hard spherical cavity surface. Denoting the potential of the two systems by V_0 and V_1, the partition function of the systems being Q_0 and Q_1, then the free energy difference between these two systems is given by

$$\beta\Delta F \equiv \beta F_1 - \beta F_0 = -\ln\frac{Q_1}{Q_0}. \tag{13}$$

By introducing a weight function $W(\mathbf{r})$, we can transform the ratio of partition functions of the two systems as [17]

$$\frac{Q_1}{Q_0} = \frac{Q_1}{Q_0}\frac{\int d\mathbf{r}W(\mathbf{r})\exp[-\beta(V_1+V_0)]}{\int d\mathbf{r}W(\mathbf{r})\exp[-\beta(V_1+V_0)]} = \frac{\langle W\exp(-\beta V_1)\rangle_0}{\langle W\exp(-\beta V_0)\rangle_1}, \tag{14}$$

where $\mathbf{r}$ represents the coordinates of all particles in the system and the subscripts 0 and 1 denote an average with respect to the Boltzmann factor of V_0 and V_1, respectively. The weight function W is arbitrary and may be chosen in such a way that the calculation effort is reduced. Following [17], we choose it as

$$W\propto\left[\frac{Q_0}{n_0}\exp(-\beta V_1)+\frac{Q_1}{n_1}\exp(-\beta V_0)\right]^{-1}, \tag{15}$$

where n_1 and n_0 are two arbitrary numbers to be determined later. Equation (14) then reduces to

$$\frac{Q_1}{Q_0} = \frac{n_0Q_1}{n_1Q_0}\frac{\left\langle\left[1+\frac{Q_1}{Q_0}\frac{n_0}{n_1}\exp[-\beta(V_0-V_1)]\right]^{-1}\right\rangle_0}{\left\langle\left[1+\frac{Q_0}{Q_1}\frac{n_1}{n_0}\exp[-\beta(V_1-V_0)]\right]^{-1}\right\rangle_1}. \tag{16}$$

By assuming $(Q_1/n_1)(n_0/Q_0)=e^{-C}$, we obtain

$$\frac{Q_1}{Q_0} = \frac{\langle f[\beta(V_1-V_0)+C]\rangle_0}{\langle f(-\beta(V_1-V_0)-C)\rangle_1}e^C, \tag{17}$$

$$\ln\frac{Q_1}{Q_0} = \ln\frac{\langle f[\beta(V_1-V_0)+C]\rangle_0}{\langle f[-\beta(V_1-V_0)-C]\rangle_1}+C; \tag{18}$$

here $f(x)=[1+\exp(x)]^{-1}$ is the Fermi function. Since n_1 and n_0 are arbitrary, this equation is valid for any constant C. By choosing an appropriate C, the calculation of ΔF can be quite conveniently performed. For the hard sphere potential, we may choose $C=0$ and get

$$\beta\Delta F = -\ln\frac{Q_1}{Q_0} = -\ln\frac{\langle f[\beta(V_1-V_0)]\rangle_0}{\langle f[-\beta(V_1-V_0)]\rangle_1} = -\ln\frac{N_{10}}{N_{01}}, \tag{19}$$

where N_{10} is the number of samples drawn out from the N simulated samples, which are generated with the potential V_0 where V_1 is not infinite; N_{01} is the number of samples drawn out from N simulated samples, which are generated with potential V_1 where V_0 is not infinite.

The procedure outlined above is used to calculate the free energy difference between two states of the system, the two states are regarded as two systems, 0 and 1, in the ARM language, and characterized, respectively, by the separations between the big sphere and the cavity surface, h_0 and h_1. It is clear that when $\Delta h=|h_1-h_0|$ is large, the numbers N_{10} and N_{01} can be very small compared to N, so that an extremely large number of configurations have to be generated to reduce the statistical errors of N_{10} and N_{01}. On the other hand, if Δh is very small, the two systems are nearly the same and the free energy difference between them can be very small, and therefore it is difficult to extract it from the subtraction of the two logarithms of N_{10} and N_{01}. In our study the value of Δh is chosen to assure that both N_{01} and

N_{10} are large and $|N_{10}-N_{01}|$ is not too small. The choice of Δh depends on the volume fraction η_s, which becomes smaller when η_s is larger.

Apart from a constant which can be specified arbitrarily in this study, the depletion potential V on the big hard sphere is just the free energy F of the system. The depletion force on the big sphere can be calculated by numerical differentiation of the depletion potential in the ARM.

IV. RESULTS AND DISCUSSION

Before presenting the results of our calculation, we first specify the system in more detail. The system is a fluid of unit-diameter ($2R_s=1$) hard spheres, inside or outside of a hard spherical cavity with radius R_c, the centers of the spheres are restricted inside of a sphere of radius R_c-R_s in the first case, and outside of the sphere of radius R_c+R_s in the second case. A single big hard sphere of radius R_b with its center at a distance R_c-R_b-h or R_c+R_b+h is apart from the cavity center (a distance R_b+h from the cavity surface), respectively, in the two cases. The force on the big sphere is a function of the radius ratios R_b/R_s, R_c/R_s and the bulk volume fraction η_s of the hard-sphere fluid. In the case of the big sphere inside of the cavity, and the cavity size is not large, we did a simulation of the whole system. We refer to this case as *exact* simulation hereafter. However, when the radius of the cavity is large enough or the big sphere is located outside of the cavity, only a portion of the whole system can be simulated. In this case we have to specify appropriate boundary conditions. We refer to this case as *inexact* simulation. In the *inexact* simulations, a portion of the system is defined in the following: periodic boundary conditions are used in the x and y directions with period L_{xy}, and a plane hard wall and a curved hard wall with radius of curvature R_c are placed at $z=L_z$ and $z=0$, respectively. The hard sphere fluid is confined in this simulation cell, and the big sphere is located at $z=R_b+h$. When R_c tends to infinity, the curved wall tends to be a plane, which corresponds to the wall-sphere model. The dimensions L_{xy} and L_z of the simulation cell are determined by the requirement that the density profile close to the surface of the big sphere is not affected by the boundaries. From calculations with different values of L_{xy} and L_z, we find that L_{xy} should be larger than $2R_b+16R_s$, and L_z should be larger than $2R_b+18R_s$.

For each given state of the cavity and the big sphere, the hard sphere fluid is sampled according to the Metropolis algorithm. Each sphere is randomly chosen and a trial displacement is accepted if the move does not result in an overlap to the hard cavity, the big hard sphere or other small spheres, and rejected otherwise. The magnitude of the random displacement is adjusted so that the overall acceptance ratio is about 0.5. We use typically 5×10^3 Monte Carlo steps (MCS) for equilibration of the systems and other 2×10^5 MCS to collect data, and the statistical errors are controlled less than 1%. The depletion potential is calculated directly from the simulated data by Eq. (19). The force calculation is a little bit involved in these simulations, which is calculated by two methods. The first one is with the use of the calculated potential, i.e., obtaining the force through numerical differentiation as outlined in the preceding section. The second is the DIM by using Eq. (3). Both methods have their corresponding merits and disadvantages. In the differential method, the calculated free energy from simulation contains statistical errors, while the numerical differentiation always has the effect of enlarging the errors. To improve our results, the calculated data are first smoothed by the spline regression method and then differentiated, and in this way we obtain satisfactory results of the force with controlled error. In the DIM, the depletion force can be calculated exactly if the contact density around the big sphere is known. However, in the Monte Carlo simulation, the density profile can only be obtained through an extrapolation procedure. The density is a function of the polar angle θ only from symmetry. In practical calculations we divide the space around the big sphere into shells of thickness d. The density of small sphere fluid in each shell as a function of θ is obtained through the simulation by simply collecting the number of times that a small sphere center enters the shell at the angle position θ. From the information collected in this way, we can obtain the average densities of small sphere fluids in a shell around the big sphere of thickness d, $2d$,..., etc. By evaluating the integral (2) with these densities, we obtain the following thickness-dependent forces:

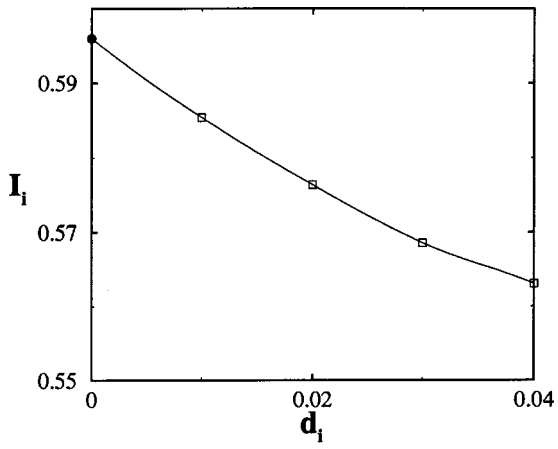

FIG. 2. Extrapolation of the integral I_i to contact $d_i=id=0$. Parameters are $R_b=5.7R_s$, $R_c=18R_s$, $h=0$, with bulk volume fraction $\eta_s=0.3$. The filled point is the extrapolated contact value.

$$I_i=\int_0^{\pi} d\theta\rho_i(\theta)\sin\theta\cos\theta. \tag{20}$$

The force can thus be obtained by extrapolating I_i to $d=0$ using the spline method. Figure 2 gives a typical process of this extrapolation where the force is plotted as a function of thickness. The extrapolation usually introduces errors.

In our system only one big hard sphere is present. We define the volume fraction of the single big hard sphere as $\eta_b=\frac{4}{3}\pi R_b^3/V$. In the exact simulations, the ratio $R_c/R_s=18$, $R_b/R_s=5.70$ so that the volume fraction $\eta_b=0.03175$. Three different volume fractions of small spheres, $\eta_s=0.1$, $\eta_s=0.2$ and $\eta_s=0.3$ were used, the num-

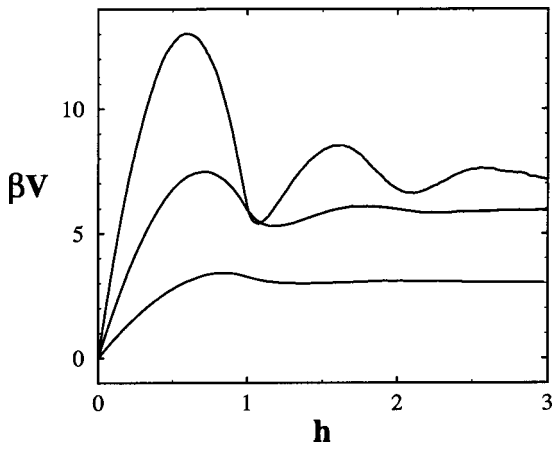

FIG. 3. Depletion potential on a big sphere inside a cavity obtained by the ARM. Parameters are $R_b=5.7R_s$, $R_c=18R_s$, with volume fractions $\eta_s=0.1$, $\eta_s=0.2$, and $\eta_s=0.3$, from bottom to top, respectively. The errors are roughly the thickness of the lines.

ber of small spheres in the three cases being 565, 1129, and 1649, respectively. Both the acceptance ratio and the small sphere densities around the big sphere are collected. The space around the big sphere is partitioned into shells of thickness $d=0.02R_s$, dividing into 180 parts along the polar angle θ with equal intervals of θ. The density around the big sphere is symmetric around the z axis so that it is independent of ϕ. The number of times that the center of small spheres enter each ring characterized by i, the label of the shell, and θ are recorded. Since the ARM can only calculate the difference of the depletion potential, we have to chose the zero point of the depletion potential. In this calculation, the depletion potential at $h=0$, where the big sphere contacts with the wall of the cavity, is set to zero as reference. However, the choice of zero point of the depletion potential has no effect on the depletion force because the force is obtained from the differentiation of the potential. In Fig. 3 the depletion potential V in units of k_BT is plotted as a function of h for three different volume fractions; it is clear that the larger volume fraction gives larger depletion effects with more structures of the depletion potential. By differentiation of the curves in Fig. 3 we obtain the depletion forces for the corresponding three cases which are plotted in Fig. 4. The estimated error in this case is smaller than the size of the symbols in the plot. We also plot in the same figure the depletion force calculated from Eq. (3) by density integral and extrapolation. It is seen from the figure that the data from the density integration method is scattered, with larger errors. The estimated largest error in this case is indicated in the figure as an error bar. As a comparison, we further plot in the figure the results of the AO approximation given by Eq. (7), which is zero when $h>2R_s$. The results obtained by the two methods are consistent, while the AO approximation underestimates the magnitude and the range of the depletion force, which also lack of the oscillatory structure.

In the inexact simulations we choose $L_{xy}=28R_s$, $L_z=29.5R_s$, and the number of small hard spheres $N_s=1548$ to maintain the volume fraction $\eta_s=0.3$ in the case where the hard sphere mixtures are inside the hard cavity, and L_{xy}

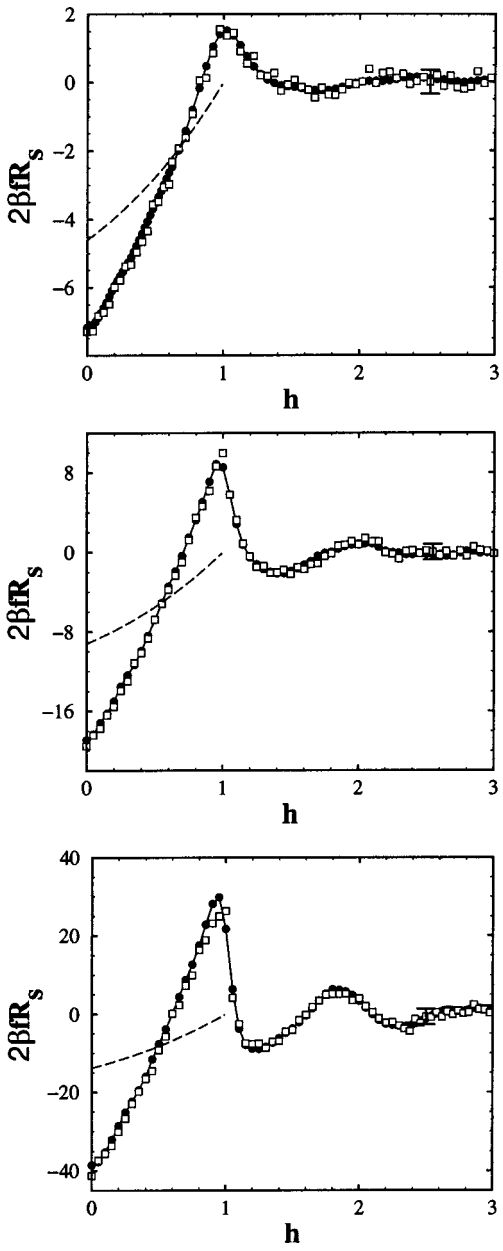

FIG. 4. Scaled depletion forces, $f^*=f/(k_BT/2R_s)$, of the same system as those in Fig. 3. Opaque squares are the results from Eq. (3), with the largest error indicated by the error bar. Filled circles (connected by the solid line) are those from the ARM, with error less than the size of the symbol. Results of the AO approximation are plotted by a dashed line for comparison.

$=28R_s$, $L_z=30.5R_s$, and $N_s=1710$ in the case where the fluid is outside the cavity. The radius of the big sphere in both cases is $R_b=5.7R_s$ and the volume fractions of the big sphere in the two cases are $\eta_b=0.03465$ and $\eta_b=0.03147$, respectively. The choice of the parameters corresponds to those in Ref. [5] for easy comparison. Figure 5 shows the depletion potential inside and outside of a hard spherical cavity. The symbols are simulation results of this work obtained with the ARM, with errors estimated less then the size of the symbols. The result obtained by the DFT in Ref. [5] is also plotted in the same figure as a solid line, and those of

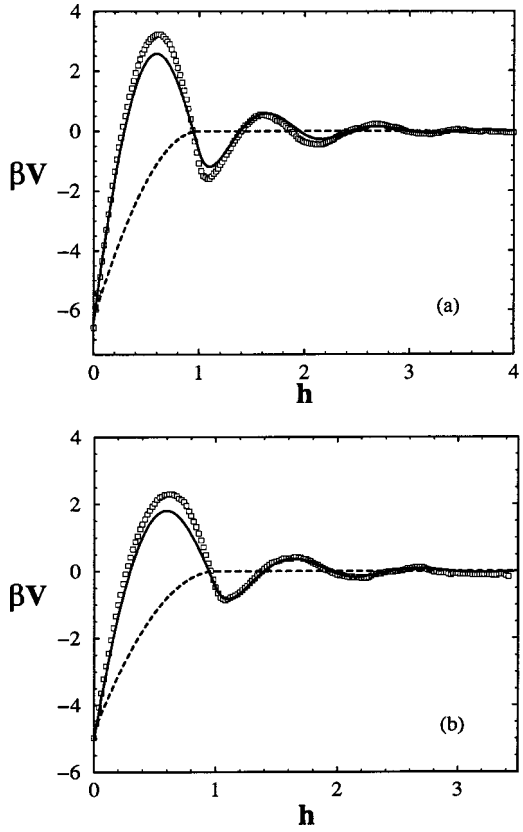

FIG. 5. Depletion potential (a) inside and (b) outside of the spherical cavity with radius $R_c=40R_s$. The radius of the big sphere is $R_b=5.7R_s$, the volume fraction is (a) $\eta_b=0.03465$ and (b) $\eta_b=0.03147$, respectively. The volume fraction of the small sphere is $\eta_s=0.3$. The symbols are obtained from simulations with the ARM, solid lines are from the density functional theory in Ref. [5], and the dashed line corresponds to the Asakura-Oosawa approximation. The errors of the simulation data are smaller than the size of the symbols.

the AO approximation as a dashed line. From Figs. 5(a) and 5(b) it can be seen that the result of the simulations and those of the DFT are in good agreement. In order to measure the difference between the simulation results and those of the DFT, we introduce a quantity ΔV_e, called the escape potential barrier in Ref. [5], defined as the difference between the maximum potential barrier and the depletion potential at contact. The simulated value of ΔV_e is $\Delta V_e^{\rm sim}=9.83$ and the value of the DFT is $\Delta V_e^{\rm dft}=8.98$ in the case of the big sphere inside the cavity. The relative error is $(\Delta V_e^{\rm sim}-\Delta V_e^{\rm dft})/\Delta V_e^{\rm dft}\approx 9\%$. By definition, the result of the DFT corresponds to the limit $\eta_b\to 0$. However, in our simulation the volume fraction of the big sphere is about 0.03, which can be one of the causes of this discrepancy. In addition, the DFT calculations are performed in the grand canonical ensemble and the density of the small spheres is fixed by the bulk chemical potential. This can introduce errors in the number density of small spheres of the system. This can be another cause of this discrepancy. The simulating value of ΔV_e is $\Delta V_e^{\rm sim}=7.28$ and that of the DFT is $\Delta V_e^{\rm dft}=6.82$ in the case of the big sphere outside the cavity. The relative error is $(\Delta V_e^{\rm sim}-\Delta V_e^{\rm dft})/\Delta V_e^{\rm dft}\approx 7\%$, slightly smaller than the first case.

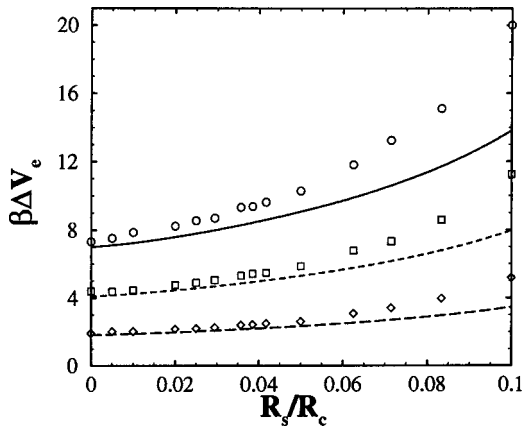

FIG. 6. Escape potential barrier $\beta\Delta V_e$ for a big sphere with radius $R_b=5R_s$ inside of a spherical cavity of radius R_c for three values of η_s. Symbols are simulation results, with errors estimated less than or about the size of the symbols (○, $\eta_s=0.3$; □, $\eta_s=0.2$; ◇, $\eta_s=0.1$). The lines are from the DFT calculations (solid line, $\eta_s=0.3$; dotted line, $\eta_s=0.2$; dashed line, $\eta_s=0.3$).

A comparison of simulation data and those of the DFT obtained by Roth *et al.* [5] for different curvatures of the cavity is shown in Fig. 6. The simulation data for R_c/R_s larger than 20 are obtained by inexact simulations; the volume fraction of the big sphere in this case is maintained to about 0.03. The data for R_c/R_s smaller than 20 are obtained with exact simulations; in this case the volume fraction of the big sphere is increased as R_c is decreased. In the figure the escape barriers of three different systems, corresponding to three volume fractions of small-sphere fluids, are plotted. The big sphere is inside the cavity, and $R_b=5R_s$. From the figure we see that when $R_c/R_s>20$, the differences between the results of the escape potential barrier $\beta\Delta V_e$ are less than 10%. At smaller ratios of R_c/R_s, the differences become larger as the ratio decreases. It should be noted that for the radius $R_c=10R_s$ of the cavity and fixed big sphere radius $R_b=5R_s$, η_b is as large as 0.125, which induces the difference between the simulation and the DFT results to 45%.

In summary, we have calculated the depletion force of a big hard sphere inside a hard spherical cavity by the Monte Carlo simulation with the ARM. The agreement of our results with those of the DFT confirms that the DFT method is effective and accurate in the calculating of the depletion potential, and it is essential to increase experimental resolution in order to measure the depletion potential using the experimental method in the future.

ACKNOWLEDGMENTS

We are grateful to R. Roth for his helpful suggestion and providing his DFT data for the depletion potential, which we include in Figs. 5 and 6. The work is supported by the National Nature Science Foundation of China and The Cheung Kong Scholars Program.

[1] S. Asakura and F. Oosawa, J. Chem. Phys. **22**, 1255 (1954).
[2] P. Attard, J. Chem. Phys. **91**, 4790 (1989).
[3] Y. Rosenfeld, Phys. Rev. Lett. **63**, 980 (1989).
[4] B. Götzelmann, R. Roth, S. Dietrich, M. Dijkstra, and R. Evans, Europhys. Lett. **47**, 398 (1999).
[5] R. Roth, B. Götzelmann, and S. Dietrich, Phys. Rev. Lett. **83**, 448 (1999).
[6] X. Ye, T. Narayanan, P. Tong, J. S. Huang, M. Y. Lin, B. L. Carvalho, and L. J. Fetters, Phys. Rev. E **54**, 6500 (1996).
[7] P. D. Kaplan, L. P. Faucheux, and A. L. Libchaber, Phys. Rev. Lett. **73**, 2793 (1994).
[8] Y. N. Ohshima, H. Sakagami, K. Okumoto, A. Tokoyoda, T. Igarashi, K. B. Shintaku, S. Toride, H. Sekino, K. Kabuto, and I. Nishio, Phys. Rev. Lett. **78**, 3963 (1997).
[9] A. D. Dinsmore, A. G. Yodh, and D. J. Pine, Nature (London) **383**, 239 (1996).
[10] A. D. Dinsmore, D. T. Wong, P. Nelson, and A. G. Yodh, Phys. Rev. Lett. **80**, 409 (1998).
[11] B. Götzelmann, R. Evans, and S. Dietrich, Phys. Rev. E **57**, 6785 (1998).
[12] Y. Mao, M. E. Cates, and H. N. W. Lekkerkerker, Physica A **222**, 10 (1995).
[13] T. Biben, P. Bladon, and D. Frenkel, J. Phys.: Condens. Matter **8**, 10799 (1996).
[14] R. Dickman, P. Attard, and V. Simonian, J. Chem. Phys. **107**, 205 (1997).
[15] J. C. Crocker, J. A. Matteo, A. D. Dinsmore, and A. G. Yodh, Phys. Rev. Lett. **82**, 4352 (1999).
[16] D. Goulding and S. Melchionna, Phys. Rev. E **64**, 011403 (2001).
[17] C. H. Bennett, J. Comput. Phys. **22**, 245 (1976); see also M. P. Allen and D. J. Tildesley, *Computer Simulation of Liquids* (Clarendon Press, Oxford, 1994), Chap. 7.